Multiscale modelling of flow, heat transfer and swelling during thermo-mechanical treatment of starch suspensions

Arnesh Palanisamy, Marco Ramaioli, Paul Menut, Artemio Plana-Fattori, Denis Flick

Multiscale modelling of flow, heat transfer and swelling during thermo-mechanical treatment of starch suspensions

Arnesh Palanisamy[a], Marco Ramaioli[a], Paul Menut[a], Artemio Plana-Fattori[a], Denis Flick[a,*]

[a] *Université Paris Saclay, INRAE, AgroParisTech, UMR SayFood, 91300, Massy, France*

Abstract

During thermal treatment of starch-based liquid food products, many coupled phenomena occur at different scales. Heat transfer affects local temperature evolution, which determines starch transformation (swelling and eventually amylose release and/or granules breakage). This transformation modifies the rheology, which in turn affects the fluid flow and heat transfer. This two-way coupling of flow, transfer and transformation was previously simulated in heat exchangers by Computational Fluid Dynamics (CFD), through purely Eulerian or Eulerian/Lagrangian approaches, assuming that the starch granules follow locally the fluid velocity. Moreover, the transformation was only characterized by a deterministic model for the mean particle size evolution (swelling). The present work takes into account directly the trajectory and the swelling of each starch granule in interaction with the surrounding fluid through an approach combining CFD with Discrete Element Method (DEM) simulations. Due to lubrication forces, the granules tend to avoid one another and when they come in contact, an elastic rebound is assumed. This approach is applied here to a waxy maize starch suspension during heating in a Couette rheometer. A shear-induced random walk of the particles is observed. Swelling first occurs near the heated wall, then swollen granules migrate toward zones of lower solid fraction. This multiscale model (rheometer scale: 1 mm, starch granule scale: 10 μm) can be used for the analysis of such rheometry tests in which the sample cannot be assumed as homogeneous.

Keywords: Starch Granule, Swelling kinetics, DEM, CFD, Modelling

*corresponding author

Email address: denis.flick@agroparistech.fr (Denis Flick)

1. Introduction

Starch is one of the most abundantly available naturally occurring biopolymers on earth. It is predominantly found in grains and tubers and is the source of 70-80 % of the calories consumed by humans worldwide in various forms of food products (Bertolini, 2010). Starch also finds many applications apart from food in industries such as bio-medical, packaging, paper, textile and pharmaceutical industries. Starch in its native form occurs as granules which consists of two polysaccharides, amylose and amylopectin. Both amylose and amylopectin have α -glucose as the monomer but differ in the way they are bonded. Amylose has α(1-4) bonds and is linear whereas amylopectin has α(1-6) bonds and is highly branched. The granule structure, molecular weight distribution, degree of amylopectin branching and the ratio of amylose to amylopectin varies according to the botanical origin of the starch granule. This, in turn, can have drastic consequences in the physical and chemical properties of the granules such as rheology and gelatinization behaviour (Banks et al., 1974; Hoover, 2001; Srichuwong et al., 2005; Visser et al., 1997). Some kinds of starch are chemically modified to have enhanced structural and functional properties of the starch granules (Debnath et al., 2013; Alcázar-Alay and Meireles, 2015). By 2025, the world starch production is projected to be around 156 million metric tons, including native and modified starches (Reportlinker.com, 2020). As a result starch has been in the past, a subject of perennial research interest for researchers from diverse backgrounds and will be in the near future as well.

Gelatinization is the process in which starch granules undergo an irreversible transformation when subjected to thermomechanical treatment in the presence of water. During this process, starch granules swell by imbibing water and the overall viscosity of the suspension increases. It is also sometimes referred to as starch pasting in literature. Starch granules are semi-crystalline with concentric rings of crystalline and amorphous phases (Ratnayake and Jackson, 2008). On the microscopic scale, the process corresponds to the melting of crystallites, loss of birefringence, leaching of amylose into the continuous phase and sometimes rupture of the granular structure (Atwell, 1988; Biliarderis, 1992). The evolution of viscos-

ity during gelatinization is also influenced by the process parameters such as concentration, shear rate, thermal history, pH and presence of other ingredients (Thomas and Atwell, 1999; Malumba et al., 2018). For high amylopectin cereal starches, such as waxy maize starch, the granules tend to hydrate with ease, swell rapidly and rupture to a great extent which results in loss of paste viscosity. As starch is used as a viscosity enhancer in many food applications such as in ketchup and also in non-food applications such as enhanced oil recovery in oil drilling, the rupture of the granules which leads to loss in suspension viscosity should be avoided, this can be avoided by chemically modifying the starch.

1.1. Coupling starch swelling, flow and heat transfer

It is of particular interest to understand the coupled evolution of temperature, starch gelatinization (notably swelling) and rheology in heat exchangers. Pioneer work was done in this field by Yang and Rao (1998) and more recently by Plana-Fattori et al. (2013) and Plana-Fattori et al. (2016). In these studies, the rheology of partially gelatinized suspension is related to the temperature evolution directly (Yang and Rao, 1998) or via a swelling kinetic model where the parameters of this model are estimated empirically. Then fluid flow and heat transfer are studied after solving the governing equations in interaction with the rheology/swelling model. The simulations were in relatively good agreement with some experimental measurement. However, these studies had several limitations: the size distribution of the granules was ignored (only average diameter evolution was considered), the variability from a granule to another in terms of swelling was ignored, the granules followed exactly the fluid flow, inside a fluid parcel (on a given trajectory) all the granules were assumed to have the same behaviour. It is known that particles migrate towards a region of lower shear rate, lower volume fraction and lower viscosity (Shauly et al., 2000). It is also known, that even without a gradient of these variables, there is shear-induced self-diffusion of the particles due to elastic collisions and lubrication interaction (Foss and Brady, 1999). This is well documented in literature (Eckstein et al., 1977; Leighton and Acrivos, 1987; Breedveld et al., 1998; Phillips et al., 1992). Shear induced self diffusivity is proportional to the shear rate and to the squared particle radius. The proportionality parameter de-

pends on the particle volume fraction (ϕ) and different correlations were proposed (linear or quadratic). Eckstein et al. (1977) found that this parameters increases almost linearly from 0 to 0.02 when the volume fraction rises from 0 to 0.2. This general trend was confirmed by Breedveld et al. (1998) who compared different studies. Inertial effect can also be involved depending on the particle Reynolds number. Also, particle migratory self-diffusion can induce an increase of momentum and heat transfer, in other words, this phenomenon can increase the apparent viscosity and conductivity.

The main question we would like to answer in this study is, are these various granular phenomena of appreciable importance in the case of starch suspension subjected to fluid flow and heat transfer? To answer this question, an approach combining Computational Fluid Dynamics (CFD) and the Discrete Element Method (DEM) is here proposed, similar to one implemented in Qian et al. (2014) for simulating granular filters. One specificity is that the suspension evolves because of the starch granule swelling. We apply this modelling approach to the case of a small gap Couette rheometer during fast heating of the external cylinder. In this case, we also have shear and heat transfer with momentum and energy exchanges between fluid and particles, possible particle migration and self-diffusion (random walk) but the fluid flow is simpler than in a heat exchanger.

1.2. Starch swelling modelling

Many models exist in the literature to predict the average degree of swelling depending on the thermal history of a given starch suspension (Lagarrigue et al., 2008; Malumba et al., 2013; Plana-Fattori et al., 2016). More recently, Desam et al. (2018a,b, 2020) proposed a mechanistic model based on the Flory-Rehner theories, for the starch swelling of various grades. However, this deals at the population level assuming same model parameters for all granules and hence, does not take into account the inter-granule variability. The inter-granule variability has biological origins and the alternating crystalline and amorphous phase of the starch granule is bound to slightly vary even among starch granules from the same plant. Thus, modelling the average behavior may not be sufficient to understand some mechanisms such as granule migration during thermal processing in presence of high velocity

and temperature gradients. Therefore, in our previous work we have described the granules swelling kinetics at the individual granule scale using a semi-mechanistic model (Palanisamy et al., 2020) for modified waxy maize starch. According to the microscopic observation of starch granules during heating in the presence of water, we observed variability in swelling kinetics from granule to granule. Each granule has a specific delay time associated with the onset of swelling. Also, the granules which began to swell at a later instant tended to swell slower compared to the granules which began to swell earlier for a given time-temperature profile. Below a minimal temperature, no swelling was observed. Experiments showed that high temperatures resulted in lower delay time and faster increase in granule diameter. These phenomena were cast mathematically in a model (Palanisamy et al., 2020). Nayouf et al. (2003) indicated that the volume fraction of granule can be estimated if the mean granule size can be accurately determined. As discussed in the next section, volume fraction of starch is a critical parameter used in the closure relations for predicting viscosity in mixture models. This inter granular level kinetic model of starch granule swelling is coupled here, with a CFD-DEM model for prediction of fluid flow, heat transfer and granule trajectories.

1.3. Starch suspension rheology

As discussed in the previous sections, starch has many different varieties and is used as a viscosity enhancer in various fields. Rheology measurements are generally carried out at a constant temperature and after complete gelatinization. However, having the evolution of rheology during gelatinization is quintessential for robust process design and can be of interest to design control strategies as well. This is done notably with the Brabender farinograph method to characterize different starches before processing. This method involves measuring the torque required to move the impeller at a predetermined rpm while measuring the temperature of the sample independently throughout the gelatinization process. However, this method does not allow measuring directly the usual rheological material functions but gives only an indication of the viscosity in arbitrary Brabender units (Eliasson, 2004). To carry out Couette rheometry of starch suspensions during heating, at a rate comparable to the industrial processes (around 1 $^{\circ}C/s$), Lagarrigue (2002) developed a high

heating/cooling rate rheometer. She took into account (via a thermal model) the thermal gradient in the rheometer gap and was able to propose a model predicting the rheology of the starch suspension as a function of its thermal history.

The properties of starch vary based on its botanical origin and processing it has undergone. Hence, suspension rheology also varies widely, it can be either shear thinning or shear thickening depending on the variety and concentrations (Plana-Fattori et al., 2016; Crawford et al., 2013). Origins of such varied behaviour of starch suspensions can be deciphered by leveraging the literature existing on viscosity predictions of broad class of materials known as non-brownian particulate suspensions.

Researchers over the years have developed two methods of modelling the suspension rheology namely, two-fluid model and mixture model (Vollebregt et al., 2010). In a two-fluid model the conservation equations are written for both particle phase and the fluid phase with the interaction terms between the phases. In the mixture approach, the suspension is modelled as an equivalent single phase. Both two-fluid model and mixture model regard the liquid and solid phases as interpenetrating continua.

The **two-fluid model** is obtained by averaging the equations of motion over the liquid and the particle phases. This results in a set of equations with a closure problem as it contains a number of indeterminate terms which are not related to the averaged variables but associated with the details in the microscopic length scale. Multiple methods exist for coming up with this closure problem. Two of which are effective medium theory and fully resolved CFD-DEM simulation. The latter is an Eulerian-Lagrangian method which is computationally expensive. Effective medium theory approach is favourable for thermodynamic and computational point of view. The indeterminate terms of the two-fluid model are represented by the effective stress tensors of the phases and interaction force exchanged by the phases. The expressions for the effective stress tensors and fluid-particle interaction forces are important as they indicate the origins of these terms.

According to Jamshidi et al. (2019), the liquid effective stress tensor is the sum of four terms. The first is the product of the liquid viscosity(μ), the liquid volume fraction (1-ϕ) and the mean liquid shear rate ($\dot{\gamma}$). The fourth term is similar to Reynolds stress and becomes

important in turbulent case. The second and third terms together are called the 'particle-particle stress'. The 'particle-presence stress' takes notably into account that the presence of particles distort the fluid streamlines and generate larger local velocity gradients, which increase viscous dissipation. This occurs even if the particles follow the liquid i.e. with zero slip velocity with the surrounding fluid. For dense mixtures, it considers also lubrication films between a significant number of particles in which viscous dissipation occurs.

For non-Brownian, neutrally buoyant, spherical particles dispersed in a Newtonian fluid in laminar flow and low volume fractions (typically $\phi < 0.05$), Jamshidi et al. (2019) recovered the expression obtained by Einstein (1905) for the part of the 'particle-presence stress' due to streamline distortion (in this derivation the lubrication interactions are neglected). Jamshidi et al. (2019) further claim that the approach often used in two-fluid modelling for the fluid/fluid interaction, which considers only the first term of the liquid effective stress tensor is incorrect and should be avoided notably because it predicts a decrease in effective viscosity as the solid concentration rises.

For dense suspensions and soft particle pastes, besides fluid/fluid interactions, a critical point is how to treat the particle/fluid and particle/particle interactions (Vollebregt et al., 2010; Van der Sman and Vollebregt, 2012). In particular, shear induced diffusion is a phenomenon of main importance. It has been shown that particle-particle interaction leads to osmotic pressure of the suspension as derived by Seth et al. (2011). These authors studied through simulations the variation of osmotic pressure and suspension shear modulus as a function of the particle properties. It was shown that gradient in osmotic pressure of a suspension contributes to the shear induced particle migration (Vollebregt et al., 2010). Further Van der Sman and Vollebregt (2012) went on to define an effective granular temperature based on osmotic pressure for sheared suspensions.

In the **mixture approach**, the suspension is considered like a single phase with an apparent viscosity also called suspension viscosity. The latter includes not only the effect of streamlines distortion due to the simple presence of the particles but also the particle/particle and fluid/particle interactions. Analytical and empirical correlations were proposed (e.g. Batchelor and Green (1972)). The four most important factors that dictate a

suspension viscosity are (a) suspending medium's viscosity, (b) granule volume fraction, (c) granule deformability, and (d) imposed shear rate (Chen et al., 2007). Granules deformability (granule's Young's modulus) is of particular importance for large volume fractions when particle-particle interactions becomes predominant (Li et al., 2020; Evans and Lips, 1990). The governing momentum equation for the mixture can also be obtained by adding the two momentum equations of the two-fluid approach, this allows also developing approximate expressions for the suspension viscosity (Jamshidi et al., 2019).

For concentrated suspensions, when fluid/fluid interactions becomes negligible compared to contact and lubrication forces, DEM simulations can also predict the rheology including shear-thickening (Ness and Sun, 2016).

Despite these efforts to understand how rheology evolution is connected to the transformation of the starch suspension during heating, there is no unequivocal single answer to explain or model all the experimentally observed phenomena.

2. Modelling

2.1. Starch swelling modelling

The previously developed individual starch granule swelling model (Palanisamy et al., 2020) is presented briefly here. In this study we use chemically stabilized cross-linked waxy maize starch (C*Tex 06205), provided by Cargil (Baupte, France). This has a D_{10} greater than 8 μm and thus is non-colloidal in nature.

For a constant reference temperature T_{ref}, the onset delay time t_{onset} follows an exponential distribution for which the cumulative distribution function is: $1 - e^{-t_{onset}/\tau_{ref}}$, where τ_{ref} is the characteristic latency time at T_{ref}. To traduce this, a parameter α called 'difficulty of swelling' was introduced. For each granule, α is selected at random from uniform distribution in the range [0;1]. This way, for constant temperature T_{ref}, the delay time t_{onset} follows:

$$t_{onset} = -\boldsymbol{\tau}_{ref} \cdot ln(1 - \alpha) \tag{1}$$

Regarding the swelling onset, equation 1 arises from an experiment carried out a constant

temperature of 62 °C during one hour (Palanisamy et al., 2020).

For variable temperature, the time delay in onset of swelling is given by solving equations 2 and 3, which means that the delay in onset of swelling is higher at lower temperatures that at higher temperatures.

$$ln(1-\alpha) = -\int_0^{t_{onset}} \frac{dt}{\tau} \tag{2}$$

$$\tau = max\left(0, \left(\frac{T_{ref} - T_{min}}{T - T_{min}}\right)\right)\tau_{ref} \tag{3}$$

Dimensionless diameter S is given by

$$S(t) = \frac{D(t) - D_i}{D_f - D_i} \tag{4}$$

where $D(t)$ is the diameter at an instant t, D_i is the initial diameter of the granule, D_f is the final diameter of the granule.

After the delay time t_{onset} is overcome, the swelling kinetics is given by:

$$\frac{dS}{dt} = K(1-S) \tag{5}$$

with

$$K = K_{ref}(1-\alpha)^{0.5}\left(\frac{T - T_{min}}{T_{ref} - T_{min}}\right)^2 \tag{6}$$

where K_{ref} is the rate constant at T_{ref} for a granule which has no difficulty to swell ($\alpha = 0$).

For chemically stabilized cross-linked waxy maize starch (C*Tex 06205) provided by Cargill (Baupte, France) the following parameters were estimated: $T_{min} = 60$ °C, $\tau_{ref} = 190$ s and $K_{ref} = 0.0023s^{-1}$ at $T_{ref} = 62$ °C. From the above equations, one can describe the swelling kinetics of these starch granules.

The following assumptions regarding the starch population were made. Initial diameters and swelling ratio are from a random normal distribution: $D_i \subset \mathcal{N}(14.77\mu m, 4.44\mu m)$, $D_f/D_i \subset \mathcal{N}(2.34, 0.33)$.

The details and experimental basis of this swelling model for individual starch granules

of cross-linked waxy maize starch were presented in previous work (Deslandes et al., 2019; Palanisamy et al., 2020). The model was validated by microscopic observation for different temperature ramps (up to 90 °C) and also by comparing size distribution obtained by Malvern mastersizer after different non-linear heat treatments. These model parameters should be re-calibrated for other waxy cross-linked starches and the model should be modified for other types of starches and is not applicable if the granule ruptures.

2.2. CFD-DEM Modelling

A two-phase modelling approach is used as by Jamshidi et al. (2019) except that the solid phase (starch granules) is not treated as a continuous phase but as a discrete one: each particle is characterized by its centre position and velocity. This approach is similar to the one used by Qian et al. (2014).

An Eulerian approach is used for solving flow and heat transfer of the continuous fluid (in this case pure water). In each representative elementary volume (REV) there are a number of solid particles (in this case starch granules).

For the fluid phase, in a general case, the momentum equation holds:

$$(1-\phi)\rho_f \frac{\partial \overrightarrow{v_f}}{\partial t} + (1-\phi)\rho_f \overrightarrow{v_f}.\overrightarrow{\nabla}\overrightarrow{v_f} = -\overrightarrow{\nabla}.\bar{\bar{S}} + (1-\phi)\rho_f \overrightarrow{g} + \overrightarrow{f_{p\to f}} \tag{7}$$

where $\overrightarrow{f_{p\to f}}$ is the sum of the forces exerted on the fluid by the particles per unit volume (notably drag forces), and $\bar{\bar{S}}$ is the fluid effective stress tensor.

For non-Brownian, neutrally bouyant, spherical particles dispersed in a Newtonian fluid in laminar flow and low volume (typically $\phi < 0.05$), Jamshidi et al. (2019) obtained the following approximation.

$$\bar{\bar{S}} = p\bar{\bar{I}} - (1+2.5\phi)\mu\bar{\bar{\dot{\gamma}}} \tag{8}$$

where $\bar{\bar{\dot{\gamma}}}$ is twice the deformation rate tensor. we can use the deformation rate tensor of the fluid because particle velocity rapidly tends to the surrounding fluid velocity (gradient of the mean particle velocity is close to the fluid velocity gradient).

In the gap of a Couette rheometer only the variations in radial directions are considered; taking a small gap, i.e. $(R_e - R_i) << R_e$, a Cartesian approximation can be used. The radial position in the gap is referred as x (unit vector $\overrightarrow{u_x}$). On the internal wall $x = 0$, on the external wall $x = e$. The flow direction is referred as y.

For the fluid, only momentum balance in y direction is considered and only the shear stress τ_{xy} is involved. Fluid velocity is assumed to be in y direction (unit vector $\overrightarrow{u_y}$) its magnitude is referred as v_f; hence:

$$(1-\phi)\rho_f \frac{\partial v_f}{\partial t} + \frac{\partial \tau_{xy}}{\partial x} = f_{y,p\to f} \tag{9}$$

where $f_{y,p\to f}$ is the sum of the forces exerted on the fluid by the particles located in the REV per unit volume in y direction. Since there is no variation in pressure nor in fluid velocity in y direction, the convective term of momentum and the pressure gradient term vanish.

In this equation τ_{xy} accounts for the fluid/fluid interaction. Therefore, this term should take into account the increased viscous dissipation due the distortion of the streamlines caused by the simple presence of the particles. According to equation 8Jamshidi et al. (2019), for dilute suspensions, it can be approximated by Einstein's correlation. Unfortunately, as per our knowledge, there is no available expression for higher volume fraction, which only integrates the additional stress due to streamlines distortion. As a case in point, the correlation of Batchelor and Green (1972) applies for higher volume fractions but includes lubrication interactions as well which are here directly calculated in the DEM part of the model. Thus, we intend to use Einstein (1905) expression for the effective viscosity even though it certainly underestimate the additional stress due to streamline distortion for intermediate solid volume fractions of $0.05 < \phi < 0.3$. At least, this relation (equation 11) takes into account that higher the particle volume fraction, the more the streamline are distorted, which increases viscous dissipation.

$$\tau_{xy} = -\mu_e(T_f, \phi)\frac{\partial v_f}{\partial x} \tag{10}$$

$$\mu_e(T,\phi) = \mu(T_f)\cdot(1+2.5\phi) \tag{11}$$

The energy balance for the fluid is :

$$(1-\phi)\rho_f C_{pf}\frac{\partial T_f}{\partial t} + \frac{\partial q}{\partial x} = Q_{p\to f} + Q_{diss} \tag{12}$$

where

$$q = -\lambda\frac{\partial T_f}{\partial x} \tag{13}$$

where $Q_{p\to f}$ is the sum of the heat fluxes from the particles to the fluid and Q_{diss} is the viscous dissipation of mechanical energy into heat due to the viscous forces.

$$Q_{diss} = \mu_e(T_f,\phi)\left(\frac{\partial v_f}{\partial x}\right)^2 \tag{14}$$

The external wall has zero velocity and imposed temperature evolution, say

$x = e : v_f = 0$ and $T_f = T_{e(t)}$.

The internal wall has a given velocity, this corresponds to a strain controlled rheometer (constant global shear rate):

$x = 0 : v_f = v_i = \dot{\gamma}.e$

The internal wall is also characterized by a given thermal inertia per unit surface ($\frac{m_{iw}C_{p.iw}}{A_{iw}}$):

$x = 0 : \frac{m_{iw}C_{p.iw}}{A_{iw}}\frac{dT_{iw}}{dt} = \lambda\frac{\partial T_f}{\partial x}$

Periodic boundary conditions apply in y and z direction.

The trajectory of each particle of index i is given by :

$$m_i\frac{d^2\overrightarrow{x_i}}{dt^2} = \overrightarrow{F_{f\to i}} + \sum_j \overrightarrow{F_{j\to i}} \tag{15}$$

with $\overrightarrow{F_{f\to i}} = 6\pi\mu r_i(v_f.\overrightarrow{u_y} - \overrightarrow{v_i})$ (Stokes viscous drag force). Here, v_f is the fluid velocity interpolated at particle centre position $\overrightarrow{x_i}$ (piecewise linear velocity profile is considered) and r_i is the radius of granule i.

The maximal observed particle/fluid relative velocity was about 1 mm/s in our case, the

maximal granule diameter is around 50 μm, and the lowest liquid viscosity is 0.32 mPa.s. Therefore, Reynolds number was always lower than 0.15, inertial effect is negligible and Stokes law is applicable. Therefore we can write that

$$F_{p\to f} = -\sum_{i\in REV} \frac{\overrightarrow{F_{f\to i}}}{V_{REV}}.\overrightarrow{u_y} \tag{16}$$

Lubrication forces in the normal direction are expressed by the following expression. Only the first-order normal force is considered, a more detailed lubrication interaction (Kim and Karrila, 2013) will be integrated in further work.

$$\overrightarrow{F_{j\to i}} = 6\pi\mu r_i \frac{\beta^2}{(1+\beta)^3}\frac{r_i + r_j}{h_{ij.eff}}((\overrightarrow{v_i} - \overrightarrow{v_j}).\overrightarrow{n_{ij}})\overrightarrow{n_{ij}} \tag{17}$$

$\overrightarrow{x_{ij}} = \overrightarrow{x_j} - \overrightarrow{x_i}$

$d_{ij} = |\overrightarrow{x_{ij}}|$

$\overrightarrow{n_{ij}} = \overrightarrow{x_{ij}}/d_{ij}$

$h_{ij} = d_{ij} - (r_i + r_j)$

$\overrightarrow{n_{ij}}$ is the centre to centre unit vector and h_{ij} is the surface to surface distance.

$h_{ij.eff} = max(h_{ij}, 0.005(r_i + r_j))$

$\beta = r_j/r_i$

No gravity, no Brownian or repulsive forces were considered.

If two particles come in contact ($h_{ij} < 0$) an instantaneous elastic rebound is assumed. Friction between particles are assumed negligible, this assumption should be reconsidered, especially for high volume fraction, since starch granules cannot be considered as smooth spheres. They exchange momentum $\overrightarrow{P}$ in the normal direction $\overrightarrow{n_{ij}}$ given by:

$$\overrightarrow{P_{j\to i}} = \frac{2m_i m_j}{m_i + m_j}((\overrightarrow{v_j} - \overrightarrow{v_i}).\overrightarrow{n_{ij}})\overrightarrow{n_{ij}} \tag{18}$$

$$m_i\delta\overrightarrow{v_i} = \overrightarrow{P_{j\to i}}; \qquad m_j\delta\overrightarrow{v_j} = \overrightarrow{P_{i\to j}} \tag{19}$$

where $\delta\overrightarrow{v_i}$ and $\delta\overrightarrow{v_j}$ are the difference in velocities before and after the collision for particles

i and j which are applied during next time step.

Elastic rebound was assumed on the internal and external walls ($x = 0$ and $x = e$). Periodic boundary conditions were assumed in y and z direction for both the particle and fluid phases.

Seth et al. (2006) have used a similar approach of elastohydrodynamic lubrication for microgels. However, they have used Hertzian contact model when particles touch each other in place of the instantaneous shocks in the model presented here. In their case with a high concentration suspension, a detailed contact model was essential because the volume fraction was higher than the random close packing fraction. In our case, the maximum volume fraction is about 30 %, much lower than the random close packing value of 68 % which was determined for our poly-disperse suspension using the methodology given in Farr and Groot (2009). Thus, the current approach (instantaneous elastic collision) seems a valid approximation.

The temperature evolution of each particle is given by:

$$m_i C_{pp} \frac{dT_i}{dt} = Q_{f \to i} + Q_{ld} \tag{20}$$

with $Q_{f \to i} = 4\pi r_i^2 h(T_f - T_i)$, $h = Nu\frac{\lambda}{2r_i}$ and $Nu \approx 2$. Here, Q_{ld} is the dissipation term for the lubrication forces and drag. The same is calculated using the following expression:

$$Q_{ld} = \frac{1}{2}\sum_j [\overrightarrow{F_{j \to i}} \cdot (\overrightarrow{v_i} - \overrightarrow{v_j})] + \overrightarrow{F_{f \to i}} \cdot (v_f \overrightarrow{u_y} - \overrightarrow{v_i}) \tag{21}$$

Initially the granules are randomly distributed, the fluid and particle velocity varies linearly in the gap and the temperature is uniform and equal to the minimal swelling temperature (60 °C)

Elsewhere researchers have often used fabric tensor to quantify anisotropy (Ness and Sun, 2016; Barreto et al., 2009). However, fabric tensor is typically used for the cases of quasi-static systems and we have a dynamic system with almost no true contacts. This is why we consider 'quasi-contact' when the centre-centre distance between particle i and j is

less than 1.2 $(r_i + r_j)$ where r_i and r_j are the radius of granules i and j. There exists two definitions of fabric tensor and multiple definitions for the fabric deviator. Here, we follow the definitions as reported in Barreto et al. (2009). They are as follows

$$\Omega_{ij} = \frac{1}{N_c} \sum_{k=1}^{N_c} n_i^k n_j^k \tag{22}$$

where N_c is the total number of quasi-contacts and n_i^k denotes the component of the normalized centre to centre vector in direction i for the k-th quasi-contact.

Thus, we have the fabric tensor which is a 3×3 matrix. The eigenvectors give the dominant directions of these quasi-contacts. The eigenvalues (Ω_1, $\Omega_2 < \Omega_1$, $\Omega_3 < \Omega_2$) are called major, intermediate and minor magnitudes of the fabric tensor. In an isotropic situation $\Omega_1 = \Omega_2 = \Omega_3$. The deviator fabric is defined by the following equation as reported in Barreto et al. (2009). The higher its value the more the configuration is anisotropic.

$$\Omega_d = \frac{1}{\sqrt{2}}[(\Omega_1 - \Omega_2)^2 + (\Omega_2 - \Omega_3)^2 + (\Omega_1 - \Omega_3)^2]^{0.5} \tag{23}$$

2.3. Numerical solving

The simulated domain was of 1 mm in x-direction ($R_e - R_i$ of the Couette rheometer) and 200 μm in the two other directions.

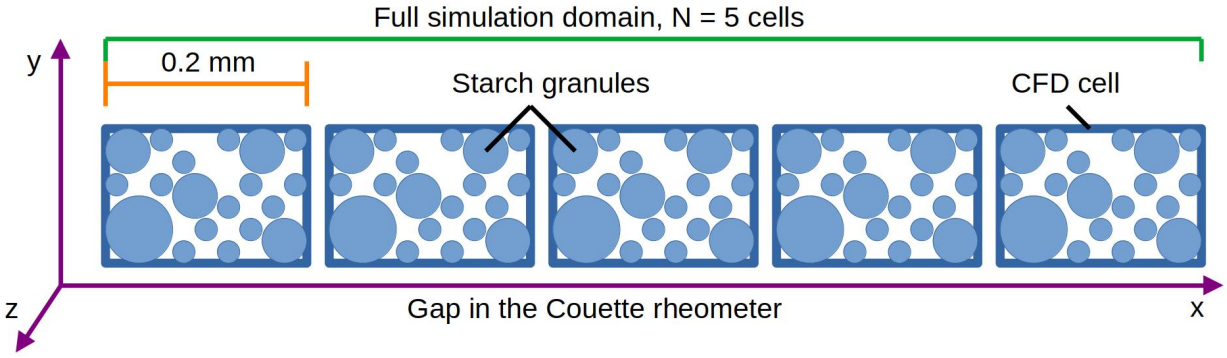

Figure 1: Simulation domain

Particle centroid method is used for coupling the DEM to the CFD. As the name sug-

gested the entire particle is assigned to a particular cell based on the location of the centroid of the particle. This method is known to be accurate only when the fluid cell size is significantly larger than the diameter of the particle. Thus, the fluid equations were solved with the finite volume method with $N = 5$ cells and initially 100 granules in each cell as a compromise. Also, if N is too low, the fluid velocity and temperature profile are not accurately represented and if N is too high, the number of granules in each cell becomes too low to be representative. To ensure periodic condition in y and z direction, for each particle at position (x,y,z) inside the domain, 4 mirror particles (same radius and velocity) were considered at $(x, y + \Delta y, z), (x, y - \Delta y, z), (x, y, z + \Delta z) and (x, y, z - \Delta z)$.

First, for each granule, its initial radius (r_0), its maximum swelling ratio (r_{max}/r_0) and its difficulty of swelling (α) are chosen from the distributions as defined in section 2.1. Then its position is randomly chosen to avoid any overlap. This is ensured by checking for overlap at every step and if overlap occurs a new position is chosen until there is no overlap. This methodology works as the initial volume fraction of the granules (ϕ) is very low.

At each time step, the swelling of each granule is calculated (according to the temperature history of the granule and difficulty of the swelling parameter) in order to re-evaluate its radius and mass. All the different forces and heat fluxes are then estimated. Finally, the velocities, temperatures (fluid and particles) and particle positions are actualized by an explicit first order scheme. Fluid velocity is assumed to be in y direction. Particle positions and velocities are calculated in 3D.

The maximum time step is dictated by the characteristic Stokes time ($\rho r^2/\mu$); $\Delta t = 10^{-5}$ s was chosen (smallest granules having radius of about 3 μm). The code was implemented in Matlab (MATLAB, 2018). For the fluid (Eulerian part), the velocity and the temperature profiles were considered as piecewise linear and an explicit first order scheme was used.

The presented results correspond mainly to one simulation of $N = 5$ cubic cells with a side length of 0.2 mm each. In each cell, 100 granules were initially randomly located. This allows comparing what happens with the granules depending on their initial position in the gap. The average shear rate was of 10 s^{-1} (internal wall velocity 10 mm/s). The precise results depend on the initial position and radius of the granules, four sets of random initial

conditions were simulated. The results were comparable and the reported analyze(trends, dominant phenomena, etc..) applies also for the other runs. A comparison between two runs for the evolution of some key variables is presented and the variability of some parameter between the four runs is also presented.

The simulation duration was of 1 min, during which the external wall temperature increased linearly from 60 to 90 °C. The mean volume fraction was initially 2.6 % and 30.0 % at the end of the simulation. If all the granules were completely swollen the volume fraction would have been 32.8 %, so on average, 91 % of the possible swelling is achieved after 1 min of heating.

The liquid properties are those of pure water:

$C_p = 4180 J.K^{-1}.kg^{-1}$

$\lambda_f = 0.6 W.m^{-1}.K^{-1}$

$\mu = 2.414\ 10^{-5}\ 10^{(247.8/(T_f+133))}$ Pa.s where T_f is in °C.

The starch gelatinization enthalpy was neglected. In fact, the enthalpy of gelatinization is less than 10 kJ per kg of dry starch (Desam et al., 2018a; Li et al., 2020), which corresponds to 0.3 kJ per kg of suspension. This is negligible compared to the sensible heat increase from 60 to 90 °C, which is about 125 kJ per kg of suspension.

2.4. Results and Discussion

Figure 2a presents at 5 different instants the temperature profile of the fluid vs position in the gap. Similarly, Figure 2b shows the temperature profile of the 500 granules and of surrounding fluid vs position in the gap at a time of 30 s from the start of simulation. The temperature of the particles is always very close to the local fluid temperature as shown in Figure 2b. This is always the case irrespective of the time. This can be explained by the very short characteristic time to reach thermal equilibrium. If we consider the energy balance of one particle (taking into account only the heat exchange with the fluid): $m_p C_{pp} \frac{dT_i}{dt} = hS(T_f - T_i)$.

A characteristic time appears as follows: $t_{th} = m_p C_{pp}/(h.S)$, where S is the surface area of the particle and h is obtained considering $Nu = 2$. This results in a t_{th} which is less

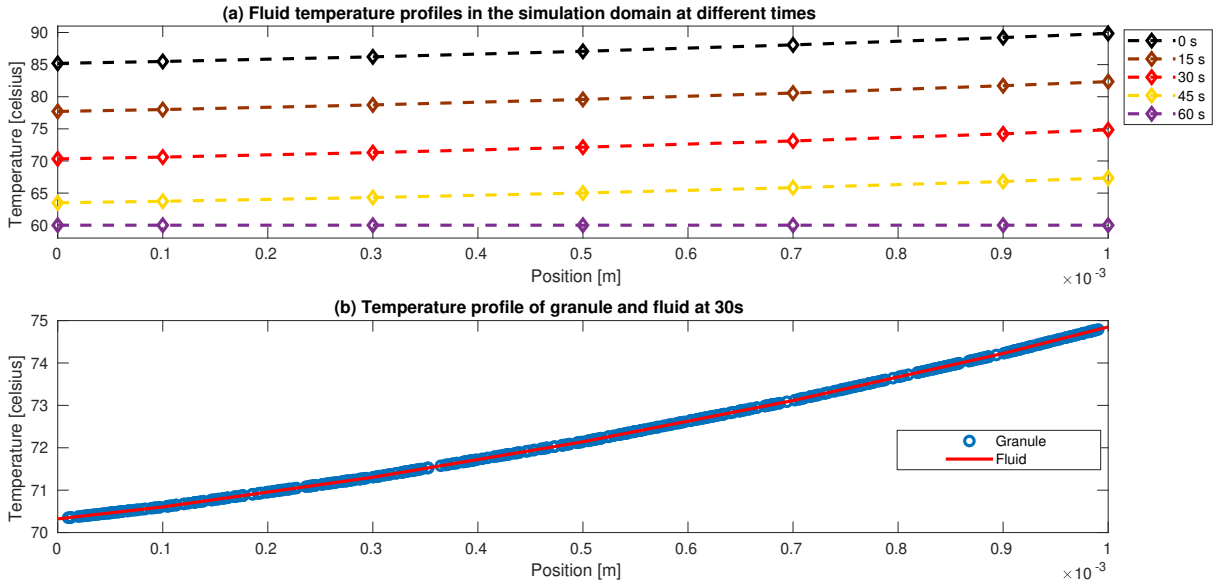

Figure 2: Temperature of granules and fluid

than 1 ms. The profile is nearly linear, the external/internal temperature difference reaches about 5 °C. The viscous dissipation of mechanical energy into heat is negligible compared to the conductive heat flux even at the end of the simulation. From Figure 7b (presented later) it appears that the dissipation is less than 0.2 W/m^3, this is much lower than the sensible heat increase of the fluid whose temperature increases by $\Delta T = 30$ °C in $\Delta t = 60$ s. In our case, $\rho_f C_{pf} \Delta T / \Delta t$ is about 2 10^6 W/m^3.

Figure 3 presents at 9 different time instants, the fluid and particles velocity profiles (v_y vs x). Cumulative particle density is superimposed, i.e. the fraction of particles whose centre is at a position lower than x. For a uniform distribution, this line would correspond to a straight line. From this we can see that near the wall there is a region where particles are absent and this region increases slightly as the swelling increases. This is arising due to the wall effects as there exists a minimum distance of particle radius between the centre of the particle and the wall (around 20 μm).

At a given time, since the curvature is ignored, the shear stress is almost constant throughout the gap, i.e. versus x in a quasi steady state approximation. This is not exactly true since the particles are growing and moving during the time, but it should apply on

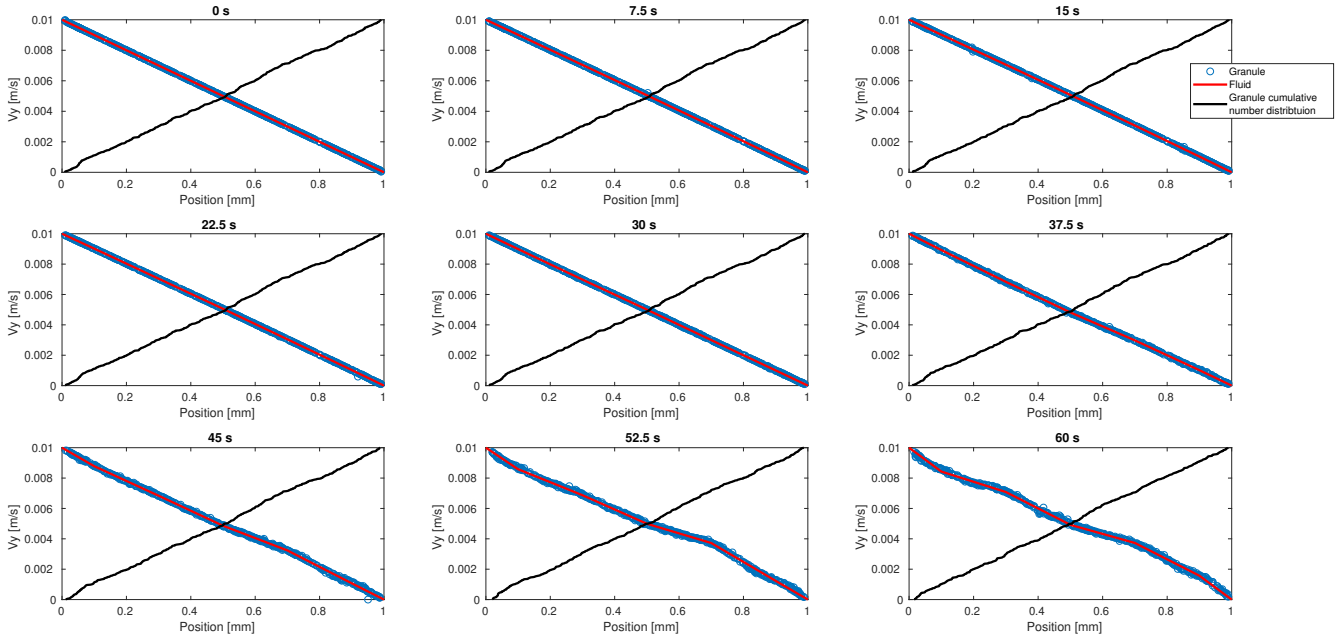

Figure 3: velocity of granules and fluid

average. Therefore, if we assume that the shear stress is almost the same across the rheometer gap, at the beginning of the simulation, one could expect a higher velocity gradient near the heated wall where the viscosity of the continuous phase is lower. This effect is observed at $t = 15$ s, the local shear rate varies monotonically between 9.8 s^{-1} to 10.2 s^{-1} from internal to an external wall. However, this variation is very small because of the limited temperature difference. At the later instances when granules swell first near the external wall, the opposite effect is expected because the suspension viscosity will be higher due to the increased volume fraction of the granules. A lower shear rate is effectively observed near the heated wall (10.7 s^{-1}) than near the internal wall (12.2 s^{-1}) at $t = 45$ s. But in the same time, the particle density decreases near the wall. This explains that the velocity gradient is higher than the average one (10 s^{-1}) near the wall and reaches its minimum value (8 s^{-1}) near the centre of the gap. This phenomenon of depletion of particles near the wall and subsequent higher shear rate is discussed in literature Coussot (2016). In addition, the interaction between a particle and the smooth wall generates no friction contrary to the

interaction between particles. This highlights that the boundary effects are not completely negligible even for a low ratio of particle diameter to gap width, which is about 4 % in our case. In future works the impact of wall lubrication forces and friction forces can be interesting to investigate. It is also observed that the particle velocity fluctuations increase with time. This is because the granules swell and occupy more volume and they interact more and more in a random manner.

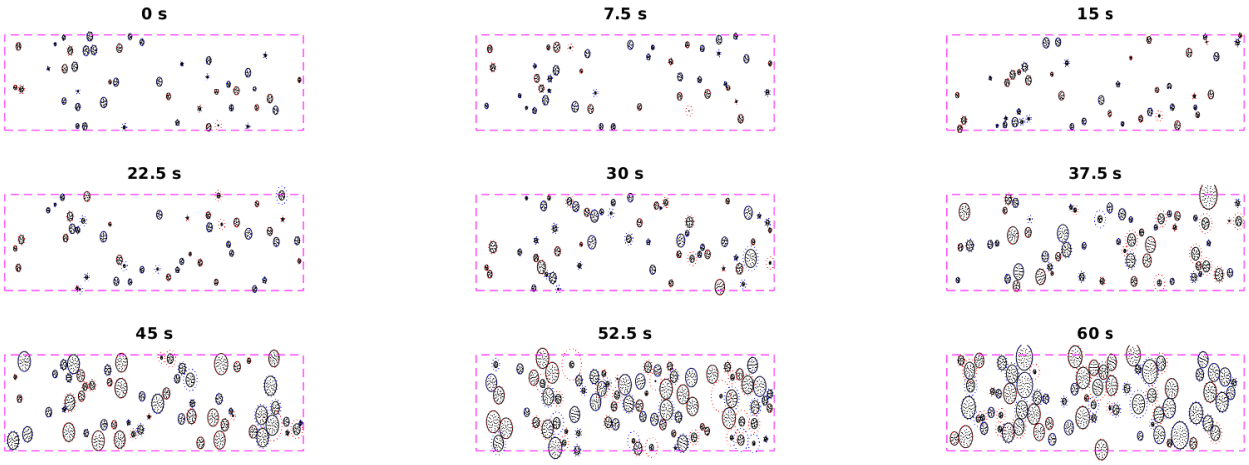

Figure 4: xy cross section of the simulation domain

Figure 4, shows a xy section (at middle z position) of the gap at 9 different instants. The granule swelling begins significantly after about 30 s. As we expected a higher degree of swelling is observed near the external heated wall (right side of the graphs) but the difference through the gap appears small, perhaps because of the particle movements. It should be noted that the swelling model was developed by observing a very dilute suspension without any motion or collision and here, we employ the same in presence of particle interactions, these interactions could modify the swelling kinetics. This should be investigated further. In the figure at 60 s, we see a small grouping of particles.

Figure 5 shows some parameters evolution as the simulation progresses. Here we show two runs of the simulation with different initial properties(radius, swelling difficulty) and positions of the starch granules (reference case at left). Figure 5a shows the evolution of

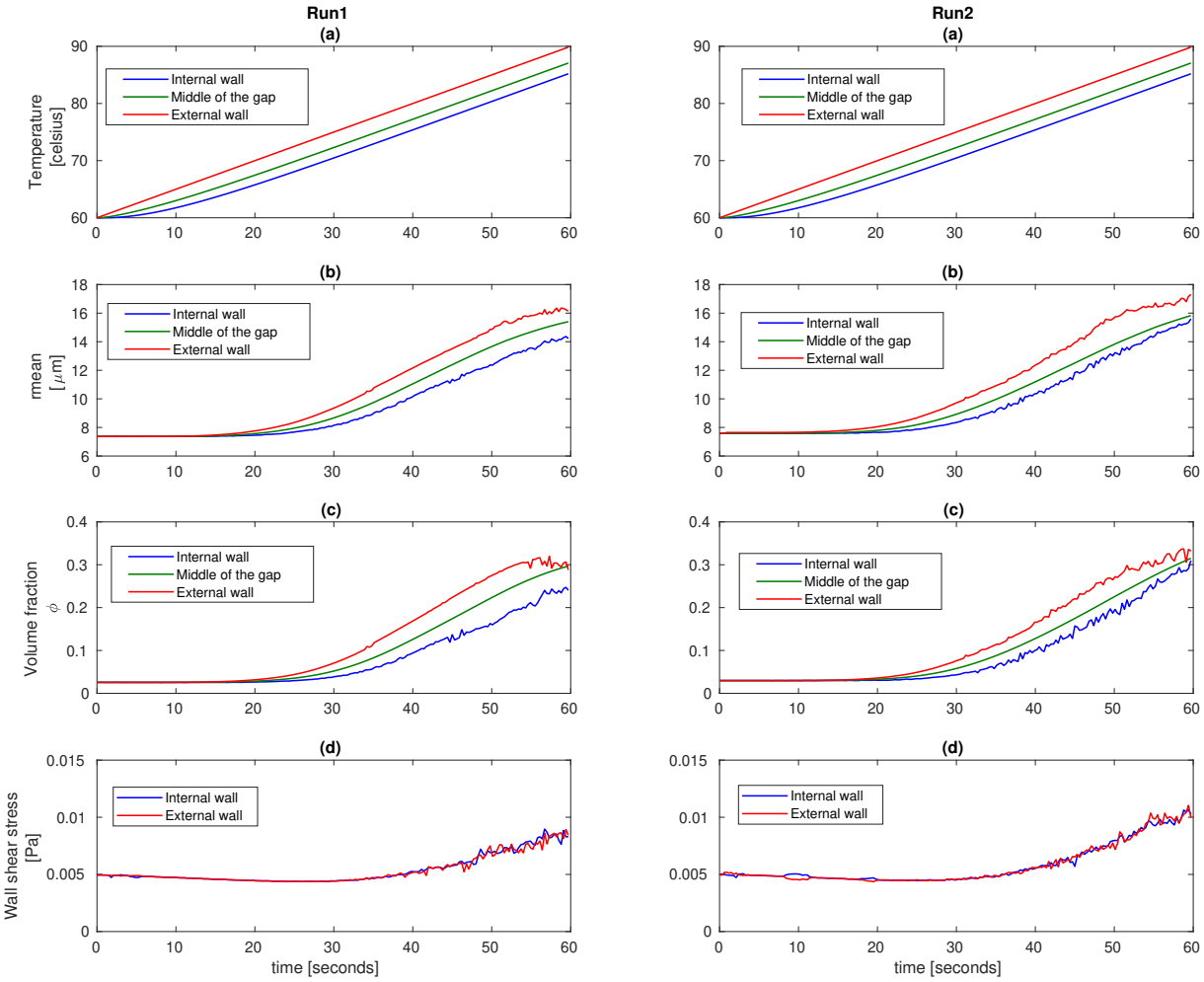

Figure 5: Time evolution of suspension parameters at different regions of the simulation domain

fluid temperature at the internal and external walls and in the middle of the gap. There is a time lag for the temperature rise from external to internal wall of about 10 s. Fig 5b presents the evolution of the mean granule radius over the entire gap, only for the internal cell and only for the external cell. The granules begin to swell significantly near the external heated wall when its temperature reaches around 70 °C. Similar to the temperature, there is also a time delay for granule swelling from the external to the internal wall. Figure 5c presents the evolution of the mean particle volume fraction ϕ over all the gap, the internal cell and the outer cell. These time series are directly related to those of granules radius. Near the heated

external wall, the volume fraction reaches a plateau whereas the mean value over the gap and the value near the internal (colder) wall are still increasing at the end of heating time of 1 min. Figure 5d shows the evolution of the wall shear stress. Shear stress first decreases slightly because when the temperature is increased, liquid viscosity decreases. But when the volume fraction reaches about 10 %, the shear stress increases significantly. The swelling effect then becomes predominant compared to liquid viscosity decrease. This stress is mainly due to the viscous friction between the fluid layers (represented here by the 5 cells). This friction is proportional to the effective viscosity which increases with the particles volume fraction. Another contribution of global stress is due to the movement of the particle relative to the fluid because of the lubrication forces and the collisions. For example, one particle located near the internal wall with a high velocity in the y-direction can move toward a more external zone, and then via the Stokes forces, it will communicate some momentum (in the y-direction) to this new fluid layer. Alternatively, it can also interact with slower particles of this layer. For a given run, the shear stress on the internal and external wall are almost equal at a given time. Random collisions can explain these fluctuations and the small differences between internal and external values. Nevertheless, averagely constant shear stress across the gap seems ensured.

From figure 5, it can be observed that the temperature evolution is the same for the two runs. The mean radius and volume fraction evolutions over the whole gap are slightly different between the two runs. This can be explained by a small difference in initial volume fraction (run 1: 2.6 % ; run 2: 2.9 %) as well as differences in swelling difficulty and swelling ratio which are randomly chosen. When we observe the internal or external cells, there are more fluctuations because of the random walk of the particles. The most important difference between the two runs is observed for the shear stress (τ_{xy}). Initially the time series are almost the same, but when swelling becomes significant ($t > 30$ s) the shear stress becomes higher for run 2. This can be explained by a slightly higher volume fraction (at the end of simulation run1: 30 %, run2: 32 %) this leads to a higher effective viscosity but also to an increase of particle/particle interactions (collisions and lubrication).

* average for 55 s $< t <$ 60 s

Table 1: Variability between runs

	$\phi_{inital}(\%)$	$\phi_{final}(\%)$	$T_{iwfinal}$ $(^\circ C)$	$\tau_{xyfinal}{}^{\star}$ (mPa)	$D^{\star}_{rwfinal}$ $(\mu m^2/s)$	$\Omega^{\star}_{d.final}$	$d_{nn.final}$ (μm)
run1	2.6	30.0	85.20	8.1	79	0.060	31.2
run2	2.9	31.5	85.20	9.9	76	0.065	31.9
run3	2.5	24.5	85.20	7.3	56	0.073	30.9
run4	2.7	30.2	85.20	8.7	82	0.067	31.2
mean	2.7	29.1	85.20	8.5	73	0.066	31.3
std	0.2	3.1	< 0.01	1.1	12	0.005	0.4

Table 1 presents the variability of some parameters between the four runs (some of them will be presented later). The variability is mainly linked to the range of initial volume fraction. For example run 3 has the lowest initial value of ϕ and logically the shear stress and the random walk diffusivity (D_{rw}) are also the lowest. Variability could be reduced by increasing box sizes in y and z direction. To compare easier different runs, the particle properties could be fixed and only the initial position could be varied. To obtain precise quantitative values, average over large number of simulations could be taken. Nevertheless the trends are the same and the phenomena analyzed of run 1 applies also to the other runs. In the following only results for run 1 are presented.

To illustrate the movement of the particles inside the gap, Figure 6d presents the time evolution of the x-displacement of 20 particles (initially 4 particles in each of the 5 cells). At the beginning of the simulation, the granules are small, they interact only weakly by lubrication forces; random walk of low amplitude is observed. After about 40 s, when the volume fraction reaches about 10 % (see Fig 5c), the grain grain interactions induce a random walk movement which becomes more significant and the displacement sometimes exceed 100 μm, which is not negligible compared to the gap width. Figure 6a presents the temperature evolution of these particles. In the beginning, the particle temperatures increase smoothly but when a random walk becomes significant, small fluctuations appear as can be observed in the zoom view in figure 6b and 6c. This means that the particle moves randomly between layers of different temperatures (more or less close to the heating wall).

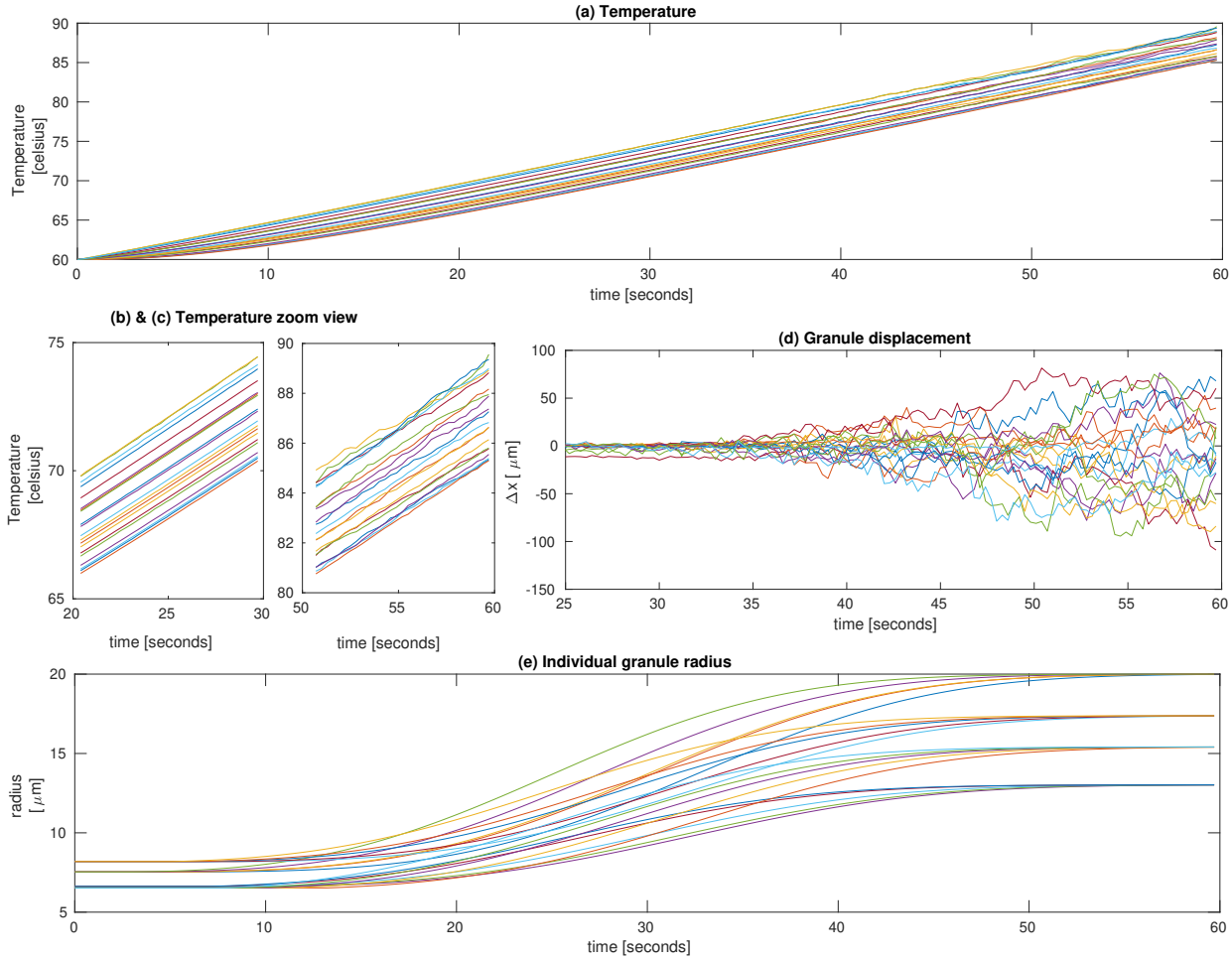

Figure 6: Sample granule properties evolution during simulation

When a particle moves towards a cold layer, heat is transferred from this particle to the fluid. This participates in heat transfer from the external to the internal wall. Figure 6e presents the radius evolution of these 20 particles. Initially, the four tracked particles in a cell have the same radius and the difficulty to swell as the four particles in the other cells to see the influence of the initial position in the gap of identical granules. As expected, the particles close to the heating wall begin to swell earlier and faster.

Figure 7a presents the variance of displacement (σ^2) in x-direction of all the particles respectively from 35 to 40 s ($\phi \approx 10$ %) and from 55 to 60 s ($\phi \approx 30$ %). For one-dimensional random walk it is expected that $\sigma^2 \approx 2D_{rw}t$ where D_{rw} is the self-diffusivity of the particles.

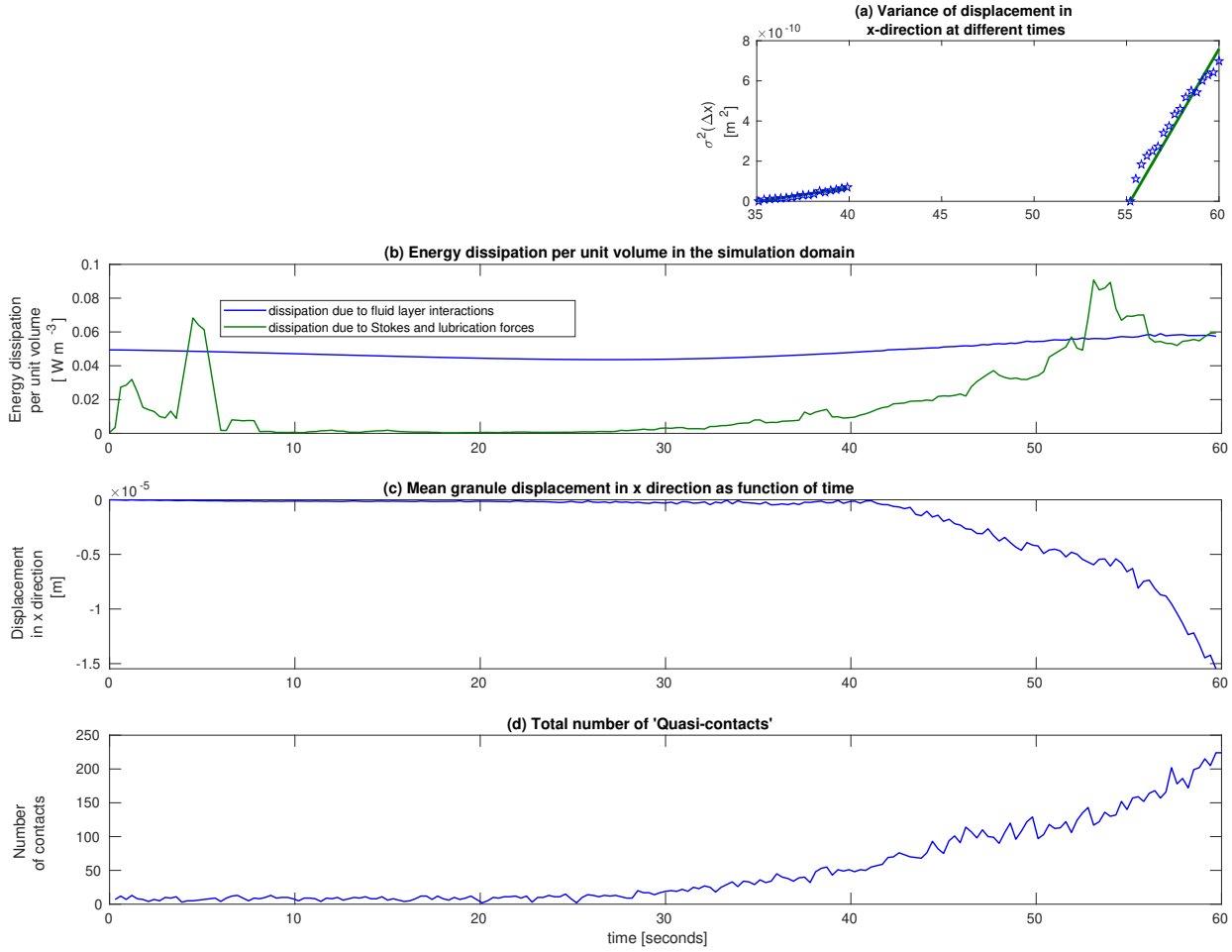

Figure 7: Granule population properties evolution with time

Different formulas are given in Leighton and Acrivos (1987), in a first approach the findings of Eckstein et al. (1977) can be used.

$$\frac{D_{rw}}{r^2\dot{\gamma}} \approx \frac{\phi}{10} \tag{24}$$

In our case $\dot{\gamma} = 10$ s^{-1}; when $\phi \approx 10$ % most of the granules are unswollen, mean radius is about 7 μm and when $\phi \approx 30$ % mean radius is about 17 μm, based on this formula the self-diffusivity is expected to be around 4.9 10^{-12} m^2/s and 8.7 10^{-11} m^2/s respectively. This is close to our estimates of D_{rw}, which is 5 10^{-12} and 1 10^{-10} m^2/s for these periods

respectively (values obtained by linear regression). This is much higher than the Brownian diffusivity of the particles due to the thermal agitation (collisions of the water molecules on the granules) $D_B = \frac{k_B T}{6\pi\mu r} \approx 5\ 10^{-14}\ \mathrm{m}^2 s^{-1}$.

The self-diffusivity due to the random walk of the particles is notably a function of the volume fraction (as shown here) and of the shear rate as shown in the literature (Leighton and Acrivos, 1987). Its value can be interesting to analyze in other situations, like heat treatment of starch suspension. For example, for a tubular heat exchanger (tube radius R_t, residence time t_r), it can reasonably be assumed that the particles follow the fluid flow only if $\sqrt{D_{rw} t_r} << R_t$.

As explained earlier, the random walk of the particles participates to heat transfer. It is expected that the apparent conductivity is increased by about $\phi \rho_p C_{pp} D_{rw}$. The order of magnitude of this additional conductivity (about 10^{-4} W.m^{-1}.K^{-1}) is however low compared to the ordinary conductivity of water (about 0.6 W.m^{-1}.K^{-1}). When this kind of heat transfer is switched off ($Nu = 0$) there is almost no difference (< 0.15 °C) in the heating rate of the internal wall.

To identify the part of the friction due to particle random walk, Figure 7b presents the evolution of the dissipation due to viscous friction between layers of fluid and the dissipation due to lubrication and drag forces (per unit volume: W.m^{-3}). The total dissipation is the product of the wall shear stress and the global shear rate. So this figure illustrates how the shear stress and similarly the mixture apparent viscosity evolve and which part is due to fluid/fluid interaction and particle/particle/fluid interactions. The fluid/fluid interaction first decreases because the liquid viscosity decreases when temperature rises. Then it increases because the solid volume fraction increases which enhances the distortion of the fluid streamlines. The particle/particle/fluid interaction (lubrication and drag) is first very low ($t < 30$ s) except at the simulation starting. Initially, due to the random localisation, some particles are very close to another, this leads to some collisions. Then the lubrication forces tend these particles to move away from each other. When the volume fraction becomes significant ($t > 30$ s) and the particles moves randomly across the gap the particle/particle interaction increases significantly the friction, or in other terms the mixture

apparent viscosity.

At the end of the simulation($\phi \approx 0.30$), the two contributions are of the same order. This highlights the importance of particle random walk in the rheology evolution of a starch suspension.

As shown previously, swelling begins near the heated wall. In addition to the random walk, a global particle migration from the zone of highest volume fraction (near the heated wall) towards zones of lower volume fraction (near the internal wall) is expected.

Figure 7c shows the mean displacement in the x-direction of the granules initially located in the cell near the heated wall vs time. The phenomenon starts effectively with the swelling but it remains small: only about 15 μm. Part of this displacement is simply due to the fact that the centre of the particles is at least one radius from the wall. This is on average 7 μm initially and 17 μm once the granules are swollen. Another part is due to diffusion in the direction opposite to the volume fraction gradient, but this gradient remains weak (Fig5c). It would be interesting in further work to relate particle migration to gradients in osmotic pressure as proposed by Vollebregt et al. (2010) but this is not easy in our case due to the heterogeneity across the gap. Thus, we can see that the granule migration towards the internal walls is significant only when the granules begin to swell. The temperature gradient and velocity gradients, which exist initially, do not lead to any significant diffusion unless the granules begin to swell.

The figure 7d shows the number of quasi contacts defined by the criteria that centre to centre distance between particles is less than $1.2\times(r_i+r_j)$. Initially when the starch granules are in an unswollen state the number of quasi-contacts are too low to determine the fabric tensor. When this number exceeded 100, the fabric deviator was found to be less than 0.1. At the end of the simulation, the fabric tensor is as follows

$$\Omega_{ij,run1} = \begin{bmatrix} 0.3549 & -0.0009 & -0.0027 \\ -0.0009 & 0.3151 & -0.0025 \\ -0.0027 & -0.0025 & 0.3300 \end{bmatrix} \tag{25}$$

and the fabric deviator, $\Omega_{d,run1} = 0.060$.

One can see very faint anisotropy based on these metrics in the system as the non-diagonal elements are very smaller than the unity. For perfect isotropy, all the non-diagonal elements are equal to zero.

The quadratic mean velocity components of the particles (relative to the fluid) in x, y and z-direction at the end of the simulation are respectively 0.097, 0.096 and 0.050 mm/s. Particle agitation is anisotropic, this can be explained by the particular direction of shear (in the velocity gradient only the term $\frac{\partial v_y}{\partial x} \neq 0$). This finding is coherent with the results of Breedveld et al. (1998) which found that the self diffusivity was 1.7 higher in the velocity gradient direction than in the other direction. A characteristic distance before direction change (like mean free path before the collision) can be obtained by dividing $2D_{rw}$ by the quadratic mean velocity. The order of magnitude is of some microns at the end of the simulation.

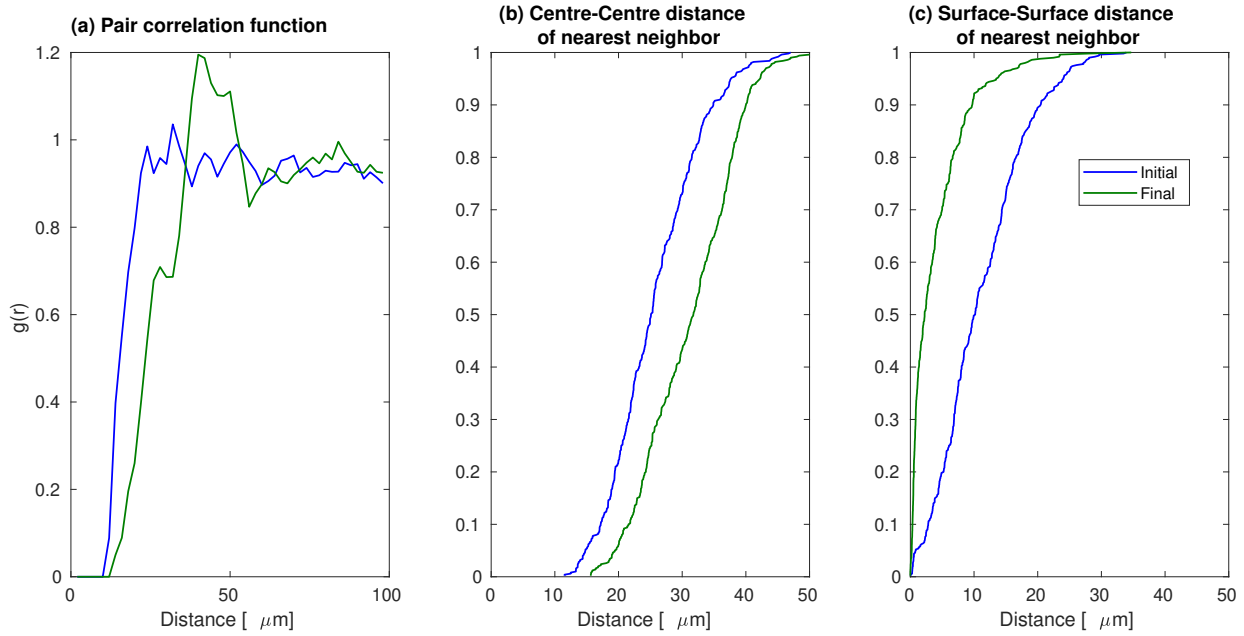

Figure 8: cumulative distributions of distance from neighbors

In figure 8a the pair correlation function or otherwise known as radial distribution function, which represents the probability of finding another particle at a given distance from

the centre of a representative particle. Initially the particles have a low volume fraction and hence the pair correlation function is fairly flat. At the end of the simulation particle swelling and increase in volume fractions lead to a peak at around 45 μm.

Figure 8b shows the cumulative distribution of the centre to the centre distance to the nearest neighbour at the beginning and the end of the simulation. The centre to centre average distance increases from 25.7 μm (initial random positioning) to 31.2 μm at the end of the simulation. The particles tend to increase their mutual distance, by the swelling effect and by the lubrication forces. However, the final value is far from the maximal possible distance (hexagonal arrangement) : $2^{1/6}(V_{box}/I)^{1/3} = 48$ μm in our case. It was mentioned previously that the particles velocity fluctuations are not isotropic. Indeed, alignment in y-direction could reduce friction (diminish dissipation) as expected from the minimal entropy production principle proposed by Prigogine (Prigogine, 1978). From the visual observation of Figure 4, such trends are not obvious even at the final instant, two zones orientated in the y-direction of lower particle density seem to be present. Therefore, to quantify possible heterogeneity/anisotropy of particles repartition in addition to the fabric tensor discussed previously, the position of the nearest neighbour of all the particles were analyzed. The root mean squared average distance to the closest neighbour of each particle in x, y and z directions at the end of the simulation are respectively 19.1, 17.5 and 18.8 μm. This indicates a small trend toward alignment in the y-direction (lower y-direction distance, higher x-direction distance). Isothermal simulations at different shear rates (not presented here) indicate that the alignment trend increases with the shear rate which could imply shear thinning. This has to be confirmed by further work. Figure 9c shows the distribution of the surface to the surface distance to the closest neighbour. The mean distance decreases from 11.1 to 4.0 μm as expected since the volume fraction increases from 2.6 to 30 %. For about 35 % of the particles, the closet neighbour is at less than 1μm at the end of the simulation.

3. Conclusion

Starch granules swelling inside a heated Couette rheometer is simulated using a CFD-DEM model with a kinetic model for granule swelling. One can see, as expected that the

sample is not uniform across the rheometer gap and the same has been quantified through various parameters. The velocity profile is not always linear except at the start of the simulation. The particle temperature is very close to the temperature of the nearby fluid always. It is also showed that random walk of the particles (self diffusivity) arising due to the lubrication force is significant. There is a small migration of particles from the outer walls to the inner cells. The transport of heat by particles is negligible compared to heat transfer by the fluid.

A small anisotropy exists in the direction of shear for the position of the particles in the system. This study was limited to a volume fraction of about 30 % whereas volume fraction up to 70 % are common in processing. For higher volume fraction, thermal effects are still expected to be negligible. However, the particle-particle and particle-fluid interaction will dominate the fluid-fluid interaction. The lubrication/drag interactions and contact frictions will gain prominence; thus, warranting a pure DEM approach by neglecting the fluid phase at ϕ close to ϕ_{rcp}. This model should be enhanced, to account for the shear-thinning behaviour which is experimentally observed for gelatinized starch suspensions of intermediate solid volume fraction. Further work could integrate full lubrication terms along with angular velocity components as well as lubrication forces between the walls and particles. In conclusion, this work gives insights into the important phenomena that one needs to consider during thermo-mechanical treatment of starch suspensions.

4. Acknowledgments

This research has been carried out with funding from European Union as part of EU RESEARCH FRAMEWORK PROGRAMME: H2020 / Marie Skłodowska-Curie Actions ITN MATHEGRAM [813202]. We acknowledge and thank the organizers of the conference Dr. Ruud Vandersman and Dr. Duynhoven John Van. We thank the participants of the conference for their comments, suggestions and inputs. Palanisamy (2021) is the conference presentation corresponding to this article.

References

Alcázar-Alay, S. C. and Meireles, M. A. A. Physicochemical properties, modifications and applications of starches from different botanical sources. *Food Science and Technology*, 35(2):215–236, 2015.

Atwell, W. The terminology and methodology associated with basic starch phenomena. *Cereal Foods World*, 33:306–311, 1988.

Banks, W., Greenwood, C., and Muir, D. Studies on starches of high amylose content. part 17. a review of current concepts. *Starch-Stärke*, 26(9):289–300, 1974.

Barreto, D., O'Sullivan, C., and Zdravkovic, L. Quantifying the evolution of soil fabric under different stress paths. In *AIP Conference Proceedings*, volume 1145, pages 181–184. American Institute of Physics, 2009.

Batchelor, G. and Green, J. The determination of the bulk stress in a suspension of spherical particles to order c2. *Journal of Fluid Mechanics*, 56(3):401–427, 1972.

Bertolini, A. C. *Trends in starch applications. Starches: Characterization, Properties, and Applications*. Taylor and Francis Group, LLC, Abingdon, 2010.

Biliarderis, C. Structure and phase transitions of starch in food system. *Food Technol.*, 46:98–109, 1992.

Breedveld, V., van den .Ende, D., Tripathi, A., and Acrivos, A. The measurement of the shear-induced particle and fluid tracer diffusivities in concentrated suspensions by a novel method. *Journal of Fluid Mechanics*, 375:297–318, 1998.

Chen, G., Campanella, O. H., and Purkayastha, S. A dynamic model of crosslinked corn starch granules swelling during thermal processing. *Journal of Food Engineering*, 81(2):500–507, 2007.

Coussot, P. *Rheophysics*. Springer, 2016.

Crawford, N. C., Popp, L. B., Johns, K. E., Caire, L. M., Peterson, B. N., and Liberatore, M. W. Shear thickening of corn starch suspensions: Does concentration matter? *Journal of colloid and interface science*, 396:83–89, 2013.

Debnath, S., Gayathri, V., and Niranjan Babu, M. Chemically modified starches and their applications in pharmacy. *International Journal of Research in Pharmaceutical and Nano Sciences*, 2(3):332–344, 2013.

Desam, G. P., Li, J., Chen, G., Campanella, O., and Narsimhan, G. A mechanistic model for swelling kinetics of waxy maize starch suspension. *Journal of Food Engineering*, 222:237–249, 2018a.

Desam, G. P., Li, J., Chen, G., Campanella, O., and Narsimhan, G. Prediction of swelling behavior of crosslinked maize starch suspensions. *Carbohydrate polymers*, 199:331–340, 2018b.

Desam, G. P., Li, J., Chen, G., Campanella, O., and Narsimhan, G. Swelling kinetics of rice and potato starch suspensions. *Journal of Food Process Engineering*, 43(4):e13353, 2020.

Deslandes, F., Plana-Fattori, A., Almeida, G., Moulin, G., Doursat, C., and Flick, D. Estimation of individual starch granule swelling under hydro-thermal treatment. *Food Structure*, 22:100125, 2019.

Eckstein, E. C., Bailey, D. G., and Shapiro, A. H. Self-diffusion of particles in shear flow of a suspension.

669 *J. Fluid Mech*, 79(1):191–208, 1977.
670 Einstein, A. *Eine neue bestimmung der moleküldimensionen*. PhD thesis, ETH Zurich, 1905.
671 Eliasson, A.-C. *Starch in food: Structure, function and applications*. CRC press, 2004.
672 Evans, I. D. and Lips, A. Concentration dependence of the linear elastic behaviour of model microgel
673 dispersions. *Journal of the Chemical Society, Faraday Transactions*, 86(20):3413–3417, 1990.
674 Farr, R. S. and Groot, R. D. Close packing density of polydisperse hard spheres. *The Journal of chemical*
675 *physics*, 131(24):244104, 2009.
676 Foss, D. R. and Brady, J. F. Self-diffusion in sheared suspensions by dynamic simulation. *Journal of fluid*
677 *mechanics*, 401:243–274, 1999.
678 Hoover, R. Composition, molecular structure, and physicochemical properties of tuber and root starches: a
679 review. *Carbohydrate polymers*, 45(3):253–267, 2001.
680 Jamshidi, R., Angeli, P., and Mazzei, L. On the closure problem of the effective stress in the eulerian-eulerian
681 and mixture modeling approaches for the simulation of liquid-particle suspensions. *Physics of Fluids*, 31
682 (1):013302, 2019.
683 Kim, S. and Karrila, S. J. *Microhydrodynamics: principles and selected applications*. Courier Corporation,
684 2013.
685 Lagarrigue, S. *Modélisation de l'évolution du comportement à l'écoulement de suspensions d'amidon soumises*
686 *à des cinétiques rapides de température et de cisaillment*. PhD thesis, Paris, Institut national d'agronomie
687 de Paris Grignon, 2002.
688 Lagarrigue, S., Alvarez, G., Cuvelier, G., and Flick, D. Swelling kinetics of waxy maize and maize starches
689 at high temperatures and heating rates. *Carbohydrate Polymers*, 73(1):148–155, 2008.
690 Leighton, D. and Acrivos, A. The shear-induced migration of particles in concentrated suspensions. *Journal*
691 *of Fluid Mechanics*, 181:415–439, 1987.
692 Li, J., Desam, G. P., Narsimhan, V., and Narsimhan, G. Methodology to predict the time-dependent storage
693 modulus of starch suspensions during heating. *Food Hydrocolloids*, page 106463, 2020.
694 Malumba, P., Jacquet, N., Delimme, G., Lefebvre, F., and Béra, F. The swelling behaviour of wheat starch
695 granules during isothermal and non-isothermal treatments. *Journal of Food Engineering*, 114(2):199–206,
696 2013.
697 Malumba, P., Doran, L., Danthine, S., Blecker, C., and Béra, F. The effect of heating rates on functional
698 properties of wheat and potato starch-water systems. *LWT*, 88:196–202, 2018.
699 MATLAB. *version 9.4.0.813654 (R2018a)*. The MathWorks Inc., Natick, Massachusetts, 2018.
700 Nayouf, M., Loisel, C., and Doublier, J. Effect of thermomechanical treatment on the rheological properties
701 of crosslinked waxy corn starch. *Journal of Food Engineering*, 59:209–219, 2003.
702 Ness, C. and Sun, J. Shear thickening regimes of dense non-brownian suspensions. *Soft matter*, 12(3):

914–924, 2016.

Palanisamy, A. Multiscale modelling of flow, heat transfer and transformation during thermal treatment of starch suspensions, July 2021. URL https://doi.org/10.5281/zenodo.5068054.

Palanisamy, A., Deslandes, F., Ramaioli, M., Menut, P., Plana-Fattori, A., and Flick, D. Kinetic modelling of individual starch granules swelling. *Food Structure*, page 100150, 2020.

Phillips, R. J., Armstrong, R. C., Brown, R. A., Graham, A. L., and Abbott, J. R. A constitutive equation for concentrated suspensions that accounts for shear-induced particle migration. *Physics of Fluids A: Fluid Dynamics*, 4(1):30–40, 1992.

Plana-Fattori, A., Chantoiseau, E., Doursat, C., and Flick, D. An eulerian–lagrangian approach for coupling fluid flow, heat transfer and liquid food product transformation. *Computers & chemical engineering*, 52: 286–298, 2013.

Plana-Fattori, A., Flick, D., Ducept, F., Doursat, C., Michon, C., and Mezdour, S. A deterministic approach for predicting the transformation of starch suspensions in tubular heat exchangers. *Journal of Food Engineering*, 171:28–36, 2016.

Prigogine, I. Time, structure, and fluctuations. *Science*, 201(4358):777–785, 1978.

Qian, F., Huang, N., Lu, J., and Han, Y. Cfd–dem simulation of the filtration performance for fibrous media based on the mimic structure. *Computers & chemical engineering*, 71:478–488, 2014.

Ratnayake, W. S. and Jackson, D. S. Starch gelatinization. *Advances in Food and Nutrition Research*, 55: 221–268, 2008.

Reportlinker.com. Global starch industry. *GLOBE NEWSWIRE, New York*, 2020.

Seth, J. R., Cloitre, M., and Bonnecaze, R. T. Elastic properties of soft particle pastes. *Journal of Rheology*, 50(3):353–376, 2006.

Seth, J. R., Mohan, L., Locatelli-Champagne, C., Cloitre, M., and Bonnecaze, R. T. A micromechanical model to predict the flow of soft particle glasses. *Nature materials*, 10(11):838–843, 2011.

Shauly, A., Wachs, A., and Nir, A. Shear-induced particle resuspension in settling polydisperse concentrated suspension. *International journal of multiphase flow*, 26(1):1–15, 2000.

Srichuwong, S., Sunarti, T. C., Mishima, T., Isono, N., and Hisamatsu, M. Starches from different botanical sources ii: Contribution of starch structure to swelling and pasting properties. *Carbohydrate Polymers*, 62(1):25–34, 2005.

Thomas, D. and Atwell, W. Eagan press handbook series: Starches. st. paul, minnesota, usa eagan press., 1999.

Van der .Sman, R. and Vollebregt, H. Effective temperature for sheared suspensions: A route towards closures for migration in bidisperse suspension. *Advances in colloid and interface science*, 185:1–13, 2012.

Visser, R. G. F., Suurs, L. C. J. M., Steeneken, P. A. M., and Jacobsen, E. Some physicochemical properties

of amylose-free potato starch. *Starch-Stärke*, 49(11):443–448, 1997.

Vollebregt, H., Van Der Sman, R., and Boom, R. Suspension flow modelling in particle migration and microfiltration. *Soft Matter*, 6(24):6052–6064, 2010.

Yang, W. and Rao, M. Numerical study of parameters affecting broken heating curve. *Journal of food engineering*, 37(1):43–61, 1998.